Research Square

Preprints are preliminary reports that have not undergone peer review.
They should not be considered conclusive, used to inform clinical practice,
or referenced by the media as validated information.

On the reactivity of the photochemically derived nitrobenzene epoxide structure with hydronium

Iván Soriano-Díaz
Universitat de València
Enrique Ortí
Universitat de València
Angelo Giussani
Angelo.Giussani@uv.es
Universitat de València

Research Article

Keywords:

Posted Date: November 25th, 2026

DOI: https://doi.org/10.21203/rs.3.rs-11726950/v1

License: This work is licensed under a Creative Commons Attribution 4.0 International License.
Read Full License

Additional Declarations: No competing interests reported.

On the reactivity of the photochemically derived nitrobenzene epoxide structure with hydronium

Iván Soriano-Díaz, Enrique Ortí, and Angelo Giussani*

Institute for Molecular Science (ICMol), Universitat de València, 46980 Paterna, Spain

Email: Angelo.Giussani@uv.es

The nitrobenzene molecule is here theoretically studied, by performing DFT, CASSCF and CASPT2 calculations, as a model of the common class of atmospheric pollutants which are nitroaromatic compounds. In particular, we focus on the possible reactivity of an intermediate epoxide structure that has been previously described to be formed as a side product of the photoreaction leading nitrobenzene to photorelease NO. The study is conducted taking into account recent researches showing that nitroaromatic compounds are suspended onto atmospheric water droplets, and that the latter constitute a significantly different environment than bulk water. Knowing that at the air-water interface atmospheric water droplets are enriched with hydronium ions, and that epoxide can undergo ring opening in acid conditions, we here study the reactivity in the presence of hydronium of the epoxide structure formed by nitrobenzene.

Introduction

Nitroaromatic compounds are a common class of atmospheric pollutants resulting from incomplete combustions.[1] They are one of the main components of the so call brown carbon aerosol present in the troposphere, which, absorbing near-ultraviolet and visible light, influences significantly the Earth's radiative balance. The characterization of the photophysics and photochemistry of nitroaromatic compounds is then fundamental in order to understand the importance and the effects of brown carbon.

Nitrobenzene (NB) is the smallest nitroaromatic molecule and is normally taken as a model to study the photophysics and photochemistry of nitroaromatic compounds. NB photophysics has been recently the subject of different studies, in some cases leading to contradictory results.[2–7] It clearly appears that the bright state (S_4) decays in an ultrafast fashion to the lowest singlet state (S_1), and that a substantial fraction of the excited state population decay into the triplet manifold, the triplet quantum yield of NB being reported to be as high as 0.8.[8] However, an ultrafast ability to decay to the ground state and/or to the triplet states remains controversial.[9–15] On the other hand, NB photochemistry has been and is still a matter of debate in the scientific community. NB can undergo three photodissociation processes: one leading to NO_2 formation, a second resulting in NO release, and a third one producing O.[16] While the relative importance of the NO_2 and NO photorelease reactions is unclear, the formation of O is considered to be a secondary path. Moreover, the photorelease of NO can occur accordingly to two different mechanisms: one along the triplet states and passing through the formation of an oxaziridine structure, the other describing a photoinduced radical roaming reaction involving both the triplet and the ground state.[10,13,17]

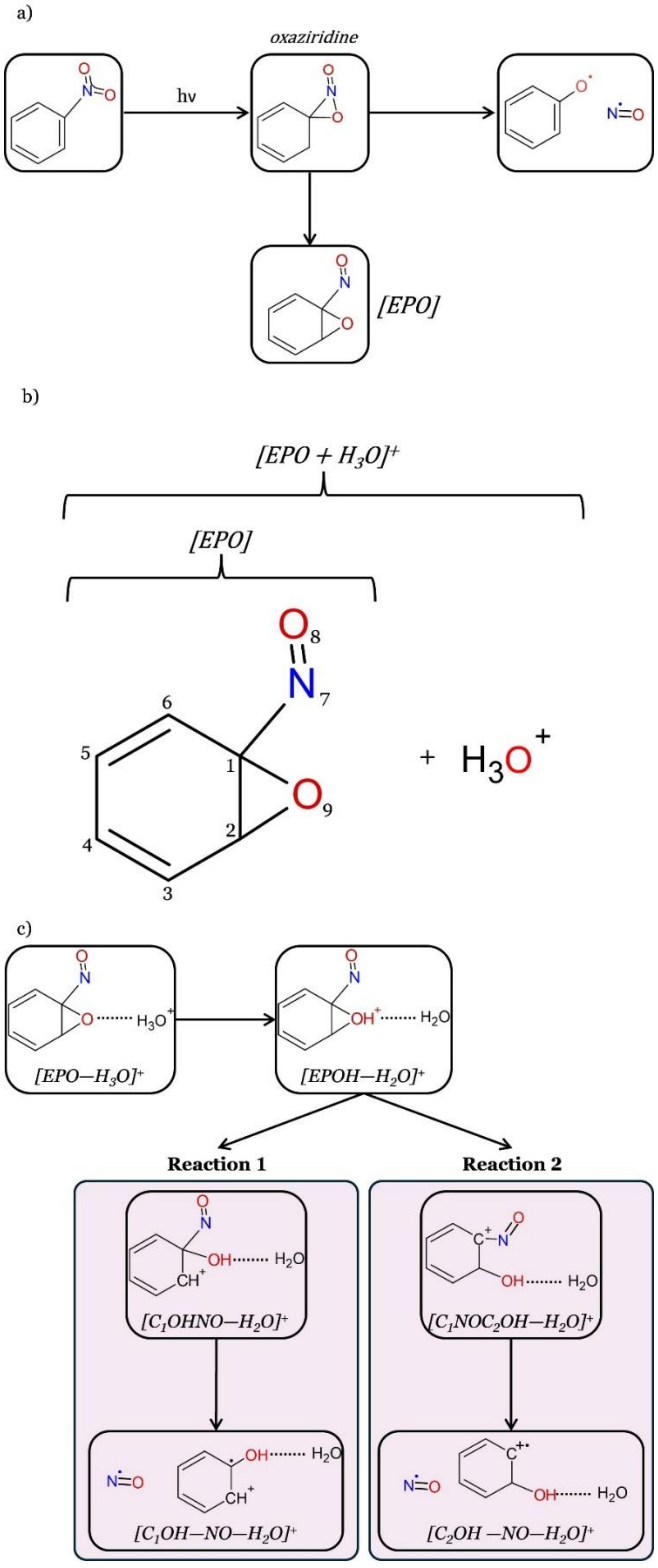
Along the first NO photorelease mechanism, one of us previously showed that from the oxaziridine ring geometry the system can also form a stable ground state epoxide structure, hereafter *EPO* (see Scheme 1a). From the latter, the system is able to release NO only through the surmounting of a substantial energy barrier, computed at the CASPT2(16,13)//CASSCF(14,11) level to be equal to 1.56 eV.[9] Such a barrier consequently makes

the formation of NO from the *EPO* structure an unfavorable process, at least for the isolated system.

NB photochemistry is particularly useful as a model for the possible photodegradation processes that nitroaromatic compounds undergo in the atmosphere. Due to the significant presence of water droplets in the troposphere, it is considered that NB is dissolved in such water droplets, which then constitute the environment where the NB photochemistry relevant for the study of brown carbon takes place. However, most of the experimental and theoretical works focus on the isolated system, with only few exceptions considering water solution.[5]

The study of reaction processes in water droplets is actually a fascinating field of research that has emerged in recent years.[18–20] Water droplets appear to be a substantially different environment than water solutions. Indeed, the kinetics of several reactions has been observed to be significantly different in water droplets with respect to water solutions. One possible factor causing such a difference could be the higher presence of radical and charged species in water droplets, and in particular at the air-water interface, which has been shown to be enriched in hydronium ions.[19]

The present contribution aims at shedding some light into the photochemistry of NB in water droplets. In particular, we analyze how the water droplet environment and its enrich hydronium concentration affects the stability of the isolated *EPO* structure. The possible chemical outputs resulting from the interaction of the *EPO* structure with the hydronium ion (see Scheme 1b) are investigated by performing accurate electronic structure calculations. First, we have evaluated the ability of hydronium to protonate the epoxide ring, and then the consequent possible ring opening. The latter was evaluated by characterizing two possible options: breaking of the C_2O_9 bond (hereafter Reaction 1) or breaking of the C_1O_9 bond (hereafter Reaction 2), as sketched in Scheme 1c.



Scheme 1. a) Formation of the epoxide structure (*EPO*) along the nitrobenzene photoinduced release of NO.[9] b) Molecular model here used as a starting point and atom labeling. c) Initially proposed reactive processes evolving from the protonated *[EPOH···H₂O]⁺* structure. The structures along Reactions 1 and 2 have been labelled stressing to which atom of the ring the NO and OH group are attached, and separating the parts of the system that are not linked by covalent bonds with hyphens.

Methods

The present contribution has been accomplished by employing different levels of electronic structure theory. In particular, DFT (Density Functional Theory), CASSCF (Complete Active Space Self-Consistent Field) and XMS-CASPT2 (Extended Multi State Complete Active Space Second Order Perturbation Theory) calculations were performed. DFT computations were done with the Orca code (version 5.0.4),[21] using the DEF2-TZVP basis set[22] and testing the PBE0, B3LYP, CAM-B3LYP, M06, ωB97X-D4 and ωB97X-V functionals.

CASSCF and XMS-CASPT2 calculations were performed with the OpenMolcas code.[23,24] The basis set ANO-R with contraction 4s3p2d1f (O, N and C) and 3s2p1d (H) was used.[25,26] Cholesky decomposition was employed to speed up the calculation of two-electron integrals.[27] Two active spaces of different size were used. A CAS(12,10) active space involving 12 active electrons distributed among 10 active orbitals was utilized to describe the initial interaction between the epoxide structure and the hydronium ion, and in particular the protonation process of the epoxide ring. Such an active space (see Figures S1 and S2) is composed of two orbitals localized on the water molecule, two π and two π* orbitals localized on the phenyl ring, two n orbitals localized on the NO group, and one π and one π* orbital also localized on the NO group. An enlarged active space of 14 electrons in 12 orbitals, CAS(14,12), was used for the study of the possible following reactions. Such an active space (see Figures S3-S5) is composed by the same type of orbitals composing the CAS(12,10) active space, plus one σ and one σ* orbital localized on the bond undergoing cleavage. The enlargement of the active space is required in order to properly describe the wanted dissociation processes. Since we are studying the breaking of two different bonds (C_2O_9 and C_1O_9, see Scheme 1b for atom labelling), two different CAS(14,12) have been used: one in which the additional σ and σ* orbitals are localized on C_2O_9, hereafter CAS(14,12)-R1 (where R1 makes reference to that is the one used to described Reaction 1, see Scheme 1c), and the other, hereafter CAS(14,12)-R2, where σ and σ* are localized on C_1O_9. CAS(14,12)-R1 and CAS(14,12)-R2 are presented in Figures S3 and S4-S5, respectively.

All CASSCF and XMS-CASPT2 calculations were performed computing two roots, with an equal weight, so to stabilize the selected active space. The extended-multistate version of CASPT2 (XMS-CASPT2) was employed to recover the missing dynamic correlation of the CASSCF results.[28] An imaginary level shift of 0.2 a.u. and an ionization-potential–electron-affinity (IPEA) shift of 0.0 a.u. were employed in all perturbative calculations.

Minima were optimized both at the CASSCF and XMS-CASPT2 levels. Liner interpolation of internal coordinates (LIICs) were sometime used as initial guess of the paths connecting minima. From the higher energy points of the LIICs, transition states (TSs) were searched at both CASSCF and XMS-CASPT2 levels. In order to characterize the path leading to a selected bond breaking, relaxed scans were performed elongating the corresponding distance. From the so obtained profile, the highest energy point was again used as starting geometry for TS optimization. Intrinsic reaction coordinate (IRC) calculations were performed to confirm that each TS is connected to the desired reactant and product minima. Frequency calculations were performed in order to confirm the nature of the optimized points.

Results and discussion

Epoxide rings are known to undergone ring opening under acid conditions. Piletic et al. studied the reaction by means of DFT calculations on a cyclic oxirane–H_3O^+–water cluster system,[29] obtaining that the process starts with the protonation of the epoxide ring. We consequently evaluate the possibility of protonating the nitrobenzene *EPO* structure as a result of its

interaction with hydronium. The optimization of the *[EPO—H_3O]$^+$* and *[EPOH—H_2O]$^+$* structures (see Scheme 1) was attempted at different levels of theory. Using DFT, independently of the functional, all optimizations ended in the *[EPO—H_3O]$^+$* geometry. Performing CASSCF(12,10) optimizations instead, all converged structures are of the type *[EPOH—H_2O]$^+$*. Only at the XMS-CASPT2(12,10) level of theory both the *[EPO—H_3O]$^+$* and *[EPOH—H_2O]$^+$* minima were obtained, hereafter *[EPO—H_3O]$^+_{min\text{-}xpt2(12,10)}$* and *[EPOH—$H_2O$]$^+_{min\text{-}xpt2(12,10)}$*, respectively (see Figure 1 and Figure S6). The two XMS-CASPT2 minima display very similar energies (see Figure 1) being the protonated epoxide structure 0.16 eV lower in energy that the unprotonated one. The energy required for the protonation process was evaluated through a LIIC calculation (see Figure 1), obtaining an energy barrier of 0.07 eV, while the inverse process requires to surmount a barrier of 0.23 eV. A frequency analysis reveals that both minima are actually displaying a small imaginary frequency equal to 164 and 173 cm^{-1} for the *[EPO—H_3O]$^+_{min\text{-}xpt2(12,10)}$* and *[EPOH—$H_2O$]$^+_{min\text{-}xpt2(12,10)}$* geometries, respectively. The imaginary frequency of *[EPO—H_3O]$^+_{min\text{-}xpt2(12,10)}$* describes a proton transfer from hydronium to the epoxide ring and to the nitrogen atom of the NO group (see Figure S7a). Meanwhile, the imaginary frequency of *[EPOH—H_2O]$^+_{min\text{-}xpt2(12,10)}$* describes a vibration of the water molecule (see Figure S7b). Altogether, these results point toward a favorable formation of the protonated epoxide structure.

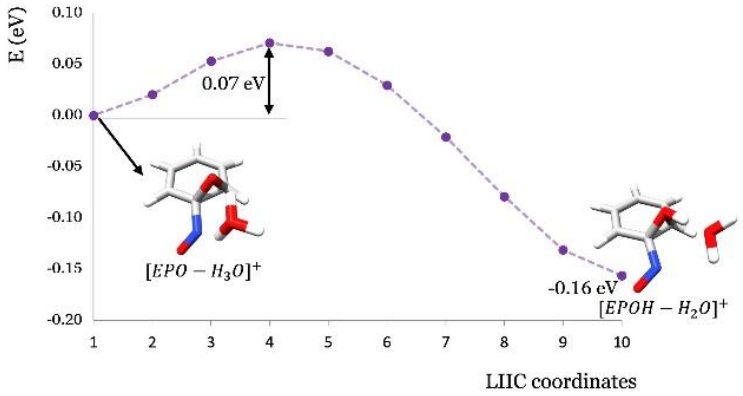


Figure 1. XMS-CASPT2(12,10) LIIC path connecting the *[EPO—H_3O]$^+_{min\text{-}xpt2(12,10)}$* and *[EPOH—$H_2O$]$^+_{min\text{-}xpt2(12,10)}$* structures.

Table 1: CASSCF(14,12), XMS-CASPT2//CASSCF(14,12), and XMS-CASPT2(14,12) relative energies (in eV) calculated for the different critical points characterized on the electronic ground state (S_0) potential energy surface. All energies are reported with respect to the S_0 energy at the *[EPOH—H_2O]$^+_{min}$* geometry for each methodology. Table S1 collects the corresponding absolute energies.

Reaction	Structure[a]	E (eV)		
		CASSCF(14,12)	XMS-CASPT2// CASSCF(14,12)	XMS-CASPT2(14,12)
1	*[EPOH—H_2O]$^+_{min}$*	0.00	0.00	0.00
	[C_1OHNO—$H_2$0]$^+_{TS}$	0.21	0.53	0.35
	[C_1OH-NO—$H_2$0]$^+_{min}$	−2.17	−2.13	−2.47
2	*[EPOH—H_2O]$^+_{min}$*	0.00	0.00	0.00
	[C_1NOC_2OH—$H_2$0]$^+_{TS}$	0.29	0.36	0.42
	[C_1NOC_2OH—$H_2$0]$^+_{min}$	−0.31	−0.01	−0.20

[a] The level of theory used to optimize the structure is CASSCF(14,12) or XMS-CASPT2(14,12) as specified in the subsequent columns.

From the *[EPOH—H_2O]$^+_{min\text{-}xpt2(12,10)}$* structure, the two proposed epoxide ring opening reactions (Reaction 1 and 2, respectively, see Scheme 1) were studied performing relaxed scans. Since DFT fails to optimize a protonated geometry, we abandoned such a method for the further characterization of the reactivity of our model. As explained in the Methods Section, the epoxide ring opening was studied with the CAS(14,12) active space, enlarged with respect to the CAS(12,10) space employed for the initial protonation step. In particular, two additional orbitals and electrons were added to the active space, corresponding to the σ and σ* orbitals of the bond whose dissociation we are willing to describe. For the description of the C_2O_9 breaking, the CAS(14,12)-R1 active space has been designed, (Figure S3) while for the description of the C_1O_9 breaking, the CAS(14,12)-R2 active space has been formed (Figures S4 and S5). In order to obtain consistent energy profiles, the [*EPOH—H_2O]$^+_{min\text{-}xpt2}$* structure was re-optimized at the CASSCF and XMS-CASPT2 level using the two CAS(14,12) active spaces. In all four optimizations (i.e., both at the CASSCF and XMS-CASPT2 levels and with both (14,12) active spaces) a minimum structure was obtained (see Figure S6), whose corresponding computed frequencies resulted all positive.

Reaction 1 was initially studied by performing a CASSCF(14,12) relaxed scan from the *[EPOH—H_2O]$^+$* optimized structure, in which the C_2O_9 bond was elongated up to 2.070 Å, a distance at which the bond can be considered broken, with steps of 0.025 Å. As shown in Figure S8a, an energy barrier of 0.25 eV is obtained along the path. Recomputing the so obtained path at the XMS-CASPT2(14,12) level (Figure S8b), the energy barrier slightly increases, reaching the value of 0.34 eV. Reoptimizing the same relaxed scan at the XMS-CASPT2 level slightly changes the obtained barrier to 0.35 eV (Figure S8c). From the last geometry of both relaxed scans, completely unconstrained optimizations were performed at the CASSCF and XMS-CASPT2 level. The latter optimizations lead to a further elongation of the C_2O_9 bond, and, more importantly, to the direct breaking of the C_1N_7 bond. The resulting optimized structures, hereafter *[C_1OH—NO—$H_2$0]$^+_{min\text{-}cas}$* and *[C_1OH—NO—$H_2$0]$^+_{min\text{-}xpt2}$*, respectively, are indeed minima, as confirmed by the computation of the corresponding frequencies, and are energetically much more stable (more than 2 eV) than the corresponding *[EPOH—H_2O]$^+_{min}$* geometry (see Table 1). Their structures are reported in Figure 2 (see also Figure S6), where it is possible to observe that the final C_1N_7 bond distance in the two minima is equal to 2.56 Å and 2.40 Å, respectively, meaning that the NO fragment, although no longer covalently bonded, is still interacting and linked to the rest of the system. Looking at the atomic Mulliken charges calculated for these structures (see Figure S9), an electrostatic interaction does not appear to be the cause of such an interaction. A possible explanation is instead the formation of a multi-centered bond between the NO radical and the phenyl carbon atoms, as it has been described in other radical cationic systems.[30–36] This hypothesis is supported by the analysis of the corresponding CASSCF wave-functions, which reveal the presence of occupied orbitals clearly describing a π–π bonding interaction between the antibonding π* orbital of the NO fragment and the phenyl ring (see Figure S10).

In order to confirm the results obtained with the relaxed scans, the TSs connecting the *[EPOH—H_2O]$^+$* and *[C_1OHC_2—NO—$H_2$0]$^+$* CASSCF and XMS-CASPT2 structures were researched. The so obtained TSs, hereafter *[C_1OHNO—$H_2$0]$^+_{TS\text{-}cas}$* and *[C_1OHNO—$H_2$0]$^+_{TS\text{-}xpt2}$*, respectively, are characterized by a single imaginary frequency of 281 and 189 cm^{-1}, indeed describing the C_2O_9 dissociation (see Figure S9). An IRC calculation further confirmed the correctness of the obtained TS. The resulting CASSCF(14,12) energy barrier for the C_2O_9 dissociation process and subsequent NO release is, employing the TS, equal to 0.21 eV (Figure 2a). Refining the energy of the CASSCF(14,12) TS geometry with XMS-CASPT2 increases significantly the barrier up to 0.53 eV (Figure 2b), while using the optimized XMS-CASPT2 structure the barrier is equal to 0.35 eV (Figure 2c).

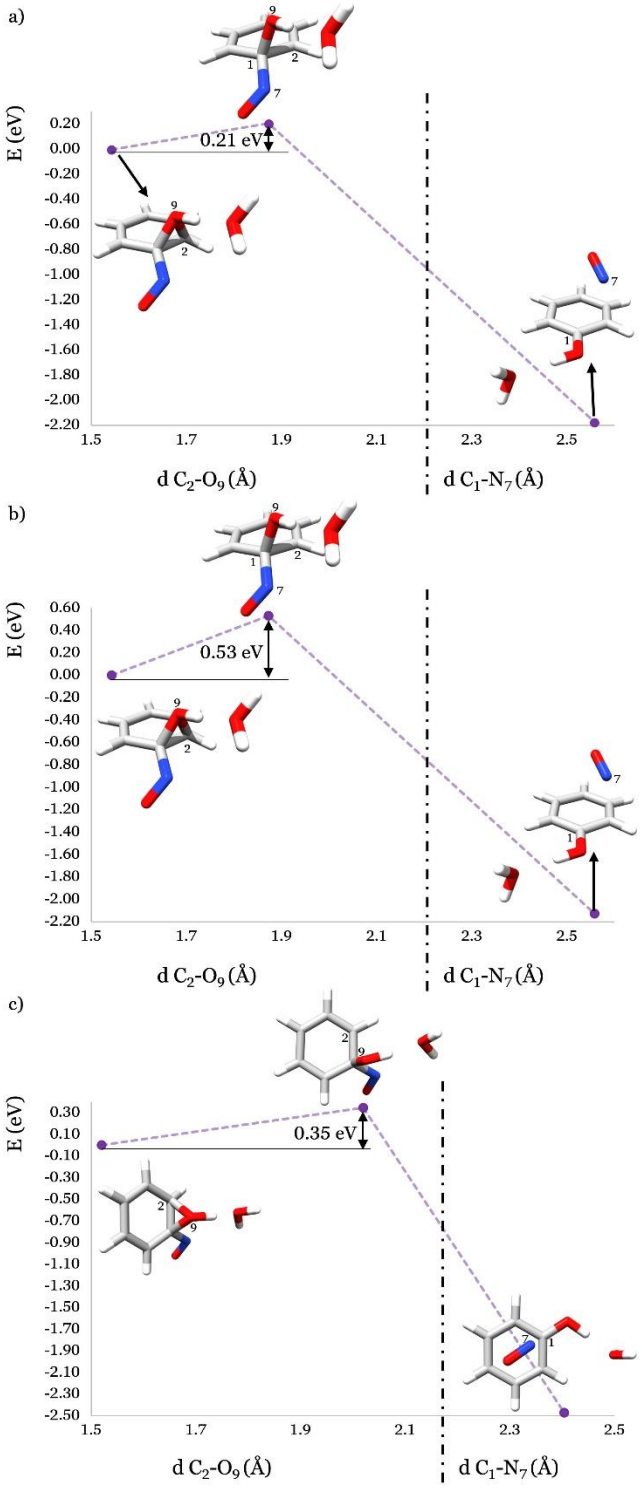


Figure 2. a) CASSCF(14,12) IRC path connecting the *[EPOH—H_2O]$^+_{min\text{-}cas}$* and *[C_1OH—NO—H_2O]$^+_{min\text{-}cas}$* structures. b) XMS-CASPT2(14,12)//CASSCF(14,12) IRC path connecting the *[EPOH—H_2O]$^+_{min\text{-}cas}$* and *[C_1OH—NO—H_2O]$^+_{min\text{-}cas}$* structures. c) XMS-CASPT2(14,12) IRC path connecting the *[EPOH—H_2O]$^+_{min\text{-}xpt2}$* and *[C_1OH—NO—H_2O]$^+_{min\text{-}xpt2}$* structures.

Regarding Reaction 2, similarly to what done for Reaction 1, it was initially studied performing a CASSCF(14,12) relaxed scan from the *[EPOH—H_2O]$^+$* optimized structure, elongating the C_1O_9 bond up to 2.063 Å, a distance at which the bond can be considered broken, with steps of 0.025 Å. As shown in Figure S10a, along the CASSCF path an energy barrier of 0.32 eV is obtained.

Recomputing the so obtained path at the XMS-CASPT2(14,12) level (Figure S10b), the energy barrier increases, reaching the value of 0.42 eV. Performing the same relaxed scan at the XMS-CASPT2 level leads to a barrier of 0.40 eV (Figure S10c). From the last geometry of both relaxed scans, completely unconstrained optimizations lead to minimum structures (*$[C_1NOC_2OH—H_20]^+_{min\text{-}cas}$* and *$[C_1NOC_2OH—H_20]^+_{min\text{-}xpt2}$*, respectively), where the epoxide ring is completely open and the NO and OH groups are attached to the ring through C_1 and C_2, respectively (see Figures 3 and S6). The energy of *$[C_1NOC_2OH—H_20]^+_{min\text{-}cas}$* is 0.31 eV more stable that the starting *$[EPOH—H_2O]^+_{min\text{-}cas}$* structure, while recomputing their energies at the XMS-CASPT2 level, the difference reduces to zero (see Table 1). The energy of *$[C_1NOC_2OH—H_20]^+_{min\text{-}xpt2}$* is 0.20 eV more stable that the starting *$[EPOH—H_2O]^+_{min\text{-}xpt2}$* geometry.

In order to confirm the results obtained with the relaxed scans, the TS connecting the *$[EPOH—H_2O]^+$* and *$[C_1NOC_2OH—H_20]^+$* structures was researched at both the CASSCF and XMS-CASPT2 level. In both cases, a TS was indeed obtained, hereafter *$[C_1NOC_2OH—H_20]^+_{TS\text{-}cas}$* and *$[C_1NOC_2OH—H_20]^+_{TS\text{-}xpt2}$*, respectively. The TS character was confirmed by computing the corresponding vibrational frequencies. Imaginary values of 203 and 283 cm^{-1} were obtained for the CASSCF and XMS-CASPT2 geometries, respectively, describing in both cases the C_1O_9 bond dissociation (see Figure S11). The energy barrier of the process evaluated using the CASSCF TS and employing CASSCF energies is equal to 0.29 eV, while refining the energies of such CASSCF structures performing single point XMS-CASPT2 calculations, it increases to 0.36 eV. Using instead the XMS-CASPT2 geometries and energies, the obtained barrier is equal to 0.42 eV.

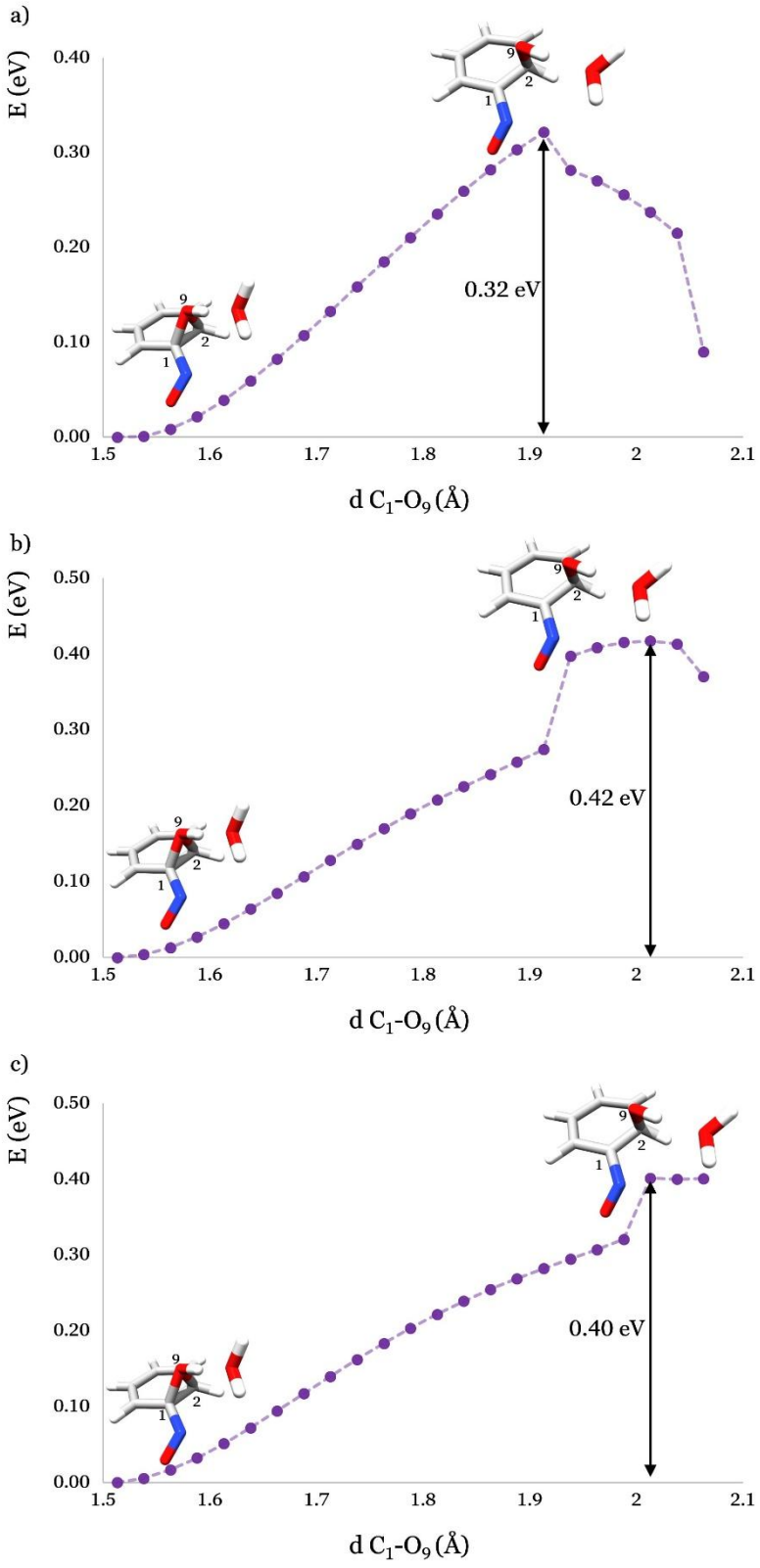
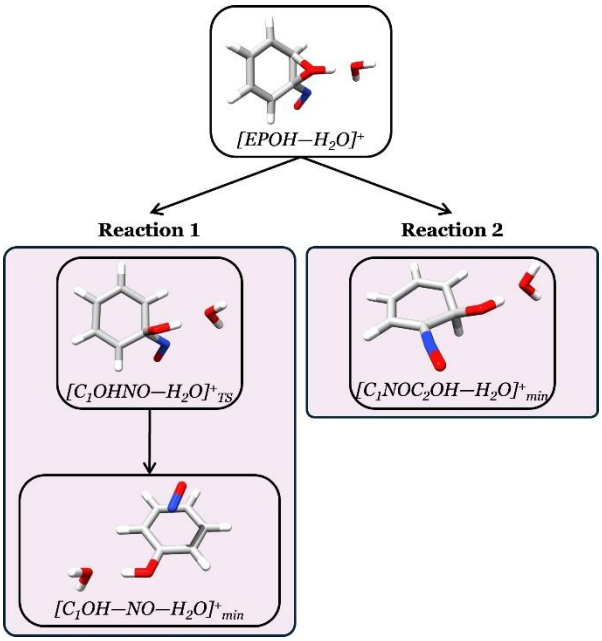


Figure 3. a) CASSCF(14,12) IRC path connecting the $[EPOH—H_2O]^+_{min\text{-}cas}$ and $[C_1NOC_2OH—H_20]^+_{min\text{-}cas}$ structures. b) XMS-CASPT2(14,12)//CASSCF(14,12) IRC path connecting the $[EPOH—H_2O]^+_{min\text{-}cas}$ and $[C_1NOC_2OH—H_20]^+_{min\text{-}cas}$ structures. c) XMS-CASPT2(14,12) IRC path connecting the $[EPOH—H_2O]^+_{min\text{-}xpt2}$ and $[C_1NOC_2OH—H_20]^+_{min\text{-}xpt2}$ structures.

To investigate the potential evolution of the system from the $[C_1NOC_2OH—H_20]^+$ structure and, in particular, the possibility of C_1N_7 dissociation, a relaxed scan elongating the C_1–N_7 distance was performed at the CASSCF(14,12) level. Along the calculated scan, all the points increase their energy with respect to the $[C_1NOC_2OH—H_20]^+_{min\text{-}cas}$ structure, then indicating an energetically non-favorable process. The same procedure repeated at the XMS-CASPT2(14,12) level did not converge.

Once characterized the two reactions, we are in the position of comparing them. The energy barriers of reactions 1 and 2 evaluated using the XMS-CASPT2 optimized structures, which can be considered as the highest level of theory, are equal to 0.35 and 0.42 eV, respectively. This makes reaction 1 slightly more energetically accessible. Moreover, the final product of Reaction 1 ($[C_1OH—NO—H_20]^+$), in which the NO molecule is released, is much more stable (by more than 2 eV, Table 1), compared to the initial protonated $[EPOH—H_2O]^+$ species, than the product of Reaction 2 (between 0.01 and 0.31 eV, depending on the level of theory), consequently making Reaction 1 thermodynamically more favorable and a much more irreversible process than Reaction 2.

Finally, we can reformulate the reaction mechanisms initially proposed in Scheme 1 at the light of the obtained results. Along Reaction 1, the protonated epoxide ring opening lead to no stable structure presenting the NO and OH groups both linked to the same position of the phenyl ring (structure $[C_1OHNO—H_20]^+$ in Scheme 1), while instead it directly evolves toward $[C_1OH—NO—H_20]^+$, a structure characterized by the detachment of the NO fragment, which, although no longer covalently linked to the system, still interacts with the phenyl ring through the formation of a multi-centered bond. Along Reaction 2 instead, a stable minimum is obtained displaying both the NO and OH groups attached to different phenyl ring positions (structure $[C_1NOC_2OH—H_20]^+$ in Scheme 1), from which the liberation of NO does not appear to be a favorable process and the proposed product $[C_2OH—NO—H_20]^+$ is not obtained. A summary of the results is presented in Scheme 2.



Scheme 2. Schematic representation of the here obtained reactivity of the initial EPO structure with hydronium.

Conclusion

In the present contribution, we evaluate how the reactivity of nitrobenzene, taken as a model of nitroaromatic air pollutants, is influenced by the high hydronium concentration reported to be present at the air-water interface of atmospheric water droplets. In particular, the effect of the interaction with hydronium ions on the stability of the photochemically derived epoxide (EPO) structure of nitrobenzene has been studied by performing ab initio electronic structure calculations. It is obtained that, in contrast to the reported stability of EPO as an isolated system,[9] the presence of hydronium leads to the protonation of the epoxide ring, from where the system can proceed towards ring opening surmounting an energy barrier of the order of 0.3−0.4 eV. The latter process can occur according to two different mechanisms, leading respectively to a system where the NO and OH groups are attached at the same ring position or at distinct positions. In the former case, the system is unstable and evolves towards partial NO release, while in the latter a stable structure displaying the NO and OH groups attached to the phenyl ring is obtained.

In conclusion, we obtain that the peculiar environment that are water droplets can significantly influence the reactivity of nitroaromatic compounds, in particular causing, through the presence of hydronium at high concentration, that otherwise relatively stable epoxide structures can easily evolve towards the formation of NO species, which can then influence the photochemistry of the atmosphere.

ACKNOWLEDGMENTS

A. G. acknowledges Grant RYC2023-044677-I, funded by MCIU/AEI/10.13039/501100011033 and FSE+ and financial support by project UV-INV_AE_4230221 funded by Universitat de València. I. S.-D. thanks Generalitat Valenciana for his Predoctoral Grant (CIACIF/2021/438). We acknowledge project PID2024-162840NB-I00 funded by MICIU/AEI/10.13039/501100011033 and FEDER, UE

References

(1) Nelson, P. O.; Thayumanavan, P.; Azizian, M. F.; Williamson, K. J. Evaluation Methodology for Environmental Impact Assessment of Industrial Wastes Used as Highway Materials: An Overview with Respect to U.S. EPA's Environmental Risk Assessment Framework. *Water Pollution* **2005**, *48*, 271–291. https://doi.org/10.1007/b11437

(2) Schalk, O.; Townsend, D.; Wolf, T. J. A.; Holland, D. M. P.; Boguslavskiy, A. E.; Szöri, M.; Stolow, A. Time-Resolved Photoelectron Spectroscopy of Nitrobenzene and Its Aldehydes. *Chem. Phys. Lett.* **2018**, *691*, 379–387. https://doi.org/10.1016/j.cplett.2017.11.011

(3) Saalbach, L.; Kotsina, N.; Crane, S. W.; Paterson, M. J.; Townsend, D. Ultraviolet Excitation Dynamics of Nitrobenzenes. *Journal of Physical Chemistry A* **2021**, *125* (33), 7174–7184. https://doi.org/10.1021/acs.jpca.1c04893

(4) Crane, S. W.; Garrow, M.; Lane, P. D.; Robertson, K.; Waugh, A.; Woolley, J. M.; Stavros, V. G.; Paterson, M. J.; Greaves, S. J.; Townsend, D. The Value of Different Experimental Observables: A Transient Absorption Study of the Ultraviolet Excitation Dynamics

Operating in Nitrobenzene. *Journal of Physical Chemistry A* **2023**, *127* (31), 6425–6436. https://doi.org/10.1021/acs.jpca.3c02654

(5) Lau, N. A.; Ghosh, D.; Bourne-Worster, S.; Kumar, R.; Whitaker, W. A.; Heitland, J.; Davies, J. A.; Karras, G.; Clark, I. P.; Greetham, G. M.; Worth, G. A.; Orr-Ewing, A. J.; Fielding, H. H. Unraveling the Ultrafast Photochemical Dynamics of Nitrobenzene in Aqueous Solution. *J. Am. Chem. Soc.* **2024**, *146* (15), 10407–10417. https://doi.org/10.1021/jacs.3c13826

(6) Shivaram, N.; Thurston, R.; Belkacem, A.; Weber, T.; Tan, L. Z.; Slaughter, D. S. Interplay between Ultrafast Electronic and Librational Dynamics in Liquid Nitrobenzene Probed with Two-Color Four-Wave Mixing. **2026**, *17*, 2911–2918. https://doi.org/10.1021/acs.jpclett.6c00102

(7) Giussani, A.; Worth, G. A. Insights into the Complex Photophysics and Photochemistry of the Simplest Nitroaromatic Compound: A CASPT2//CASSCF Study on Nitrobenzene. *J. Chem. Theory Comput.* **2017**, *13* (6), 2777–2788. https://doi.org/10.1021/acs.jctc.6b01149

(8) Takezaki, M.; Hirota, N.; Terazima, M. Nonradiative Relaxation Processes and Electronically Excited States of Nitrobenzene Studied by Picosecond Time-Resolved Transient Grating Method. *Journal of Physical Chemistry A* **1997**, *101* (19), 3443–3448. https://doi.org/10.1021/jp963095t

(9) Giussani, A.; Worth, G. A. How Important Is Roaming in the Photodegradation of Nitrobenzene? *Physical Chemistry Chemical Physics* **2020**, *22* (28), 15945–15952. https://doi.org/10.1039/d0cp02077j

(10) Bejoy, N. B.; Roy Chowdhury, P.; Patwari, G. N. Modulating the Roaming Dynamics for the NO Release in Ortho-Nitrobenzenes. *Journal of Physical Chemistry Letters* **2023**, *14* (11), 2816–2822. https://doi.org/10.1021/acs.jpclett.3c00134

(11) Liu, R.; Zhang, Z.; Yan, L.; Yang, X.; Zhu, Y.; Su, P.; Song, H.; Wang, Z. The Influence of Hydrogen Bonds on the Roaming Reaction. *Journal of Physical Chemistry Letters* **2023**, *14* (41), 9351–9356. https://doi.org/10.1021/acs.jpclett.3c02133

(12) Giussani, A.; Worth, G. A. On the Photorelease of Nitric Oxide by Nitrobenzene Derivatives: A CASPT2//CASSCF Model. *Journal of Chemical Physics* **2022**, *157* (20). https://doi.org/10.1063/5.0125460

(13) Giussani, A.; Worth, G. A. A First Proposal on the Nitrobenzene Photorelease Mechanism of NO2 and Its Relation to NO Formation through a Roaming Mechanism. *Journal of Physical Chemistry Letters* **2024**, *15* (8), 2216–2221. https://doi.org/10.1021/acs.jpclett.3c03457

(14) Hegazy, K.; Bucksbaum, P.; Centurion, M.; Cryan, J.; Li, R.; Lin, M. F.; Moore, B.; Nunes, P.; Shen, X.; Weathersby, S.; Yang, J.; Wang, X.; Wolf, T. Tracking Dissociation Pathways of Nitrobenzene via Mega-Electron-Volt Ultrafast Electron Diffraction. *Journal of Physics B: Atomic, Molecular and Optical Physics* **2024**, *57* (19). https://doi.org/10.1088/1361-6455/ad7431

(15) Lam, C. S.; Chou, T. C.; McManus, J.; Hodgkinson, C.; Burt, M.; Brouard, M. The Femtochemistry of Nitrobenzene Following Excitation at 240 Nm. *Commun. Chem.* **2025**, *8* (1). https://doi.org/10.1038/s42004-025-01672-2

(16) Galloway, D. B.; Bartz, J. A.; Huey, L. G.; Crim, F. F. Pathways and Kinetic Energy Disposal in the Photodissociation of Nitrobenzene. *J. Chem. Phys.* **1993**, *98* (3), 2107–2114. https://doi.org/10.1063/1.464188

(17) Hause, M. L.; Herath, N.; Zhu, R.; Lin, M. C.; Suits, A. G. Roaming-Mediated Isomerization in the Photodissociation of Nitrobenzene. *Nat. Chem.* **2011**, *3* (12), 932–937. https://doi.org/10.1038/nchem.1194

(18) Ruiz-Lopez, M. F.; Francisco, J. S.; Martins-Costa, M. T. C.; Anglada, J. M. Molecular Reactions at Aqueous Interfaces. *Nature Reviews Chemistry*. Nature Research September 1, 2020, pp 459–475. https://doi.org/10.1038/s41570-020-0203-2

(19) de la Puente, M.; Laage, D. How the Acidity of Water Droplets and Films Is Controlled by the Air-Water Interface. *J. Am. Chem. Soc.* **2023**, *145* (46), 25186–25194. https://doi.org/10.1021/jacs.3c07506

(20) Qiu, L.; Cooks, R. G. Spontaneous Oxidation in Aqueous Microdroplets: Water Radical Cation as Primary Oxidizing Agent. *Angewandte Chemie - International Edition*. John Wiley and Sons Inc April 22, 2024. https://doi.org/10.1002/anie.202400118

(21) Neese, F. Software Update: The ORCA Program System–Version 5.0. *Wiley Interdiscip Rev. Comput. Mol. Sci.* **2022**, *12* (5), e1606.

(22) Weigend, F.; Ahlrichs, R. Balanced Basis Sets of Split Valence, Triple Zeta Valence and Quadruple Zeta Valence Quality for H to Rn: Design and Assessment of Accuracy. *Physical Chemistry Chemical Physics* **2005**, 3297–3305. https://doi.org/10.1039/b508541a

(23) Fdez. Galván, I.; Vacher, M.; Alavi, A.; Angeli, C.; Aquilante, F.; Autschbach, J.; Bao, J. J.; Bokarev, S. I.; Bogdanov, N. A.; Carlson, R. K.; Chibotaru, L. F.; Creutzberg, J.; Dattani, N.; Delcey, M. G.; Dong, S. S.; Dreuw, A.; Freitag, L.; Frutos, L. M.; Gagliardi, L.; Gendron, F.; Giussani, A.; González, L.; Grell, G.; Guo, M.; Hoyer, C. E.; Johansson, M.; Keller, S.; Knecht, S.; Kovačević, G.; Källman, E.; Li Manni, G.; Lundberg, M.; Ma, Y.; Mai, S.; Malhado, J. P.; Malmqvist, P. Å.; Marquetand, P.; Mewes, S. A.; Norell, J.; Olivucci, M.; Oppel, M.; Phung, Q. M.; Pierloot, K.; Plasser, F.; Reiher, M.; Sand, A. M.; Schapiro, I.; Sharma, P.; Stein, C. J.; Sørensen, L. K.; Truhlar, D. G.; Ugandi, M.; Ungur, L.; Valentini, A.; Vancoillie, S.; Veryazov, V.; Weser, O.; Wesołowski, T. A.; Widmark, P. O.; Wouters, S.; Zech, A.; Zobel, J. P.; Lindh, R. OpenMolcas: From Source Code to Insight. *J. Chem. Theory Comput.* **2019**, *15* (11), 5925–5964. https://doi.org/10.1021/acs.jctc.9b00532

(24) Li Manni, G.; Fdez. Galván, I.; Alavi, A.; Aleotti, F.; Aquilante, F.; Autschbach, J.; Avagliano, D.; Baiardi, A.; Bao, J. J.; Battaglia, S.; Birnoschi, L.; Blanco-González, A.; Bokarev, S. I.; Broer, R.; Cacciari, R.; Calio, P. B.; Carlson, R. K.; Carvalho Couto, R.; Cerdán, L.; Chibotaru, L. F.; Chilton, N. F.; Church, J. R.; Conti, I.; Coriani, S.; Cuéllar-Zuquin, J.; Daoud, R. E.; Dattani, N.; Decleva, P.; de Graaf, C.; Delcey, M. G.; De Vico, L.; Dobrautz, W.; Dong, S. S.; Feng, R.; Ferré, N.; Filatov(Gulak), M.; Gagliardi, L.; Garavelli, M.; González, L.; Guan, Y.; Guo, M.; Hennefarth, M. R.; Hermes, M. R.; Hoyer, C. E.; Huix-Rotllant, M.; Jaiswal, V. K.; Kaiser, A.; Kaliakin, D. S.; Khamesian, M.; King, D. S.;

Kochetov, V.; Krośnicki, M.; Kumaar, A. A.; Larsson, E. D.; Lehtola, S.; Lepetit, M. B.; Lischka, H.; López Ríos, P.; Lundberg, M.; Ma, D.; Mai, S.; Marquetand, P.; Merritt, I. C. D.; Montorsi, F.; Mörchen, M.; Nenov, A.; Nguyen, V. H. A.; Nishimoto, Y.; Oakley, M. S.; Olivucci, M.; Oppel, M.; Padula, D.; Pandharkar, R.; Phung, Q. M.; Plasser, F.; Raggi, G.; Rebolini, E.; Reiher, M.; Rivalta, I.; Roca-Sanjuán, D.; Romig, T.; Safari, A. A.; Sánchez-Mansilla, A.; Sand, A. M.; Schapiro, I.; Scott, T. R.; Segarra-Martí, J.; Segatta, F.; Sergentu, D. C.; Sharma, P.; Shepard, R.; Shu, Y.; Staab, J. K.; Straatsma, T. P.; Sørensen, L. K.; Tenorio, B. N. C.; Truhlar, D. G.; Ungur, L.; Vacher, M.; Veryazov, V.; Voß, T. A.; Weser, O.; Wu, D.; Yang, X.; Yarkony, D.; Zhou, C.; Zobel, J. P.; Lindh, R. The OpenMolcas Web: A Community-Driven Approach to Advancing Computational Chemistry. *J. Chem. Theory Comput.* **2023**, *19*, 6933–6991. https://doi.org/10.1021/acs.jctc.3c00182

(25) Widmark, P. O.; Malmqvist, P. Å.; Roos, B. O. Density Matrix Averaged Atomic Natural Orbital (ANO) Basis Sets for Correlated Molecular Wave Functions - I. First Row Atoms. *Theor. Chim. Acta* **1990**, *77* (5), 291–306. https://doi.org/10.1007/BF01120130

(26) Pierloot, K.; Dumez, B.; Widmark, P.-O.; Roos, B. O. Density Matrix Averaged Atomic Natural Orbital (ANO) Basis Sets for Correlated Molecular Wave Functions. *Theor. Chim. Acta* **1995**, *90* (2), 87. https://doi.org/10.1007/s002140050063

(27) Pedersen, T. B.; Aquilante, F.; Lindh, R. Density Fitting with Auxiliary Basis Sets from Cholesky Decompositions. *Theor. Chem. Acc.* **2009**, *124* (1–2), 1–10. https://doi.org/10.1007/s00214-009-0608-y

(28) Granovsky, A. A. Extended Multi-Configuration Quasi-Degenerate Perturbation Theory: The New Approach to Multi-State Multi-Reference Perturbation Theory. *Journal of Chemical Physics* **2011**, *134* (21), 1–14. https://doi.org/10.1063/1.3596699

(29) Piletic, I. R.; Edney, E. O.; Bartolotti, L. J. A Computational Study of Acid Catalyzed Aerosol Reactions of Atmospherically Relevant Epoxides. *Physical Chemistry Chemical Physics* **2013**, *15* (41), 18065–18076. https://doi.org/10.1039/c3cp52851k

(30) Tian, Y. H.; Sumpter, B. G.; Du, S.; Huang, J. Pancake π-π Bonding Goes Double: Unexpected 4e/All-Sites Bonding in Boron- and Nitrogen-Doped Phenalenyls. *Journal of Physical Chemistry Letters* **2015**, *6* (12), 2318–2325. https://doi.org/10.1021/acs.jpclett.5b00857

(31) Milašinović, V.; Krawczuk, A.; Molčanov, K.; Kojić-Prodić, B. Two-Electron Multicenter Bonding (âPancake Bonding') in Dimers of 5,6-Dichloro-2,3-Dicyanosemiquinone (DDQ) Radical Anions. *Cryst. Growth Des.* **2020**, *20* (8), 5435–5443. https://doi.org/10.1021/acs.cgd.0c00658

(32) Molčanov, K.; Jelsch, C.; Landeros, B.; Hernández-Trujillo, J.; Wenger, E.; Stilinović, V.; Kojić-Prodić, B.; Escudero-Adán, E. C. Partially Covalent Two-Electron/Multicentric Bonding between Semiquinone Radicals. *Cryst. Growth Des.* **2019**, *19* (1), 391–402. https://doi.org/10.1021/acs.cgd.8b01484

(33) Piccoli, P. M. B.; Schultz, A. J.; Sparkes, H. A.; Howard, J. A. K.; Arif, A. M.; Dawe, L. N.; Miller, J. S. [MeNC5H5]2[TCNE]2 (TCNE = Tetracyanoethylene). Single Crystal X-Ray and Neutron Diffraction Characterization of an Exceptionally Long 2.8 Å C-C Bond. *CrystEngComm* **2009**, *11* (4), 686–690. https://doi.org/10.1039/b816817b

(34) Tian, Y. H.; Kertesz, M. Is There a Lower Limit to the Cc Bonding Distances in Neutral Radical ϕ-Dimers? The Case of Phenalenyl Derivatives. *J. Am. Chem. Soc.* **2010**, *132* (31), 10648–10649. https://doi.org/10.1021/ja103396h

(35) Abdulla, H. M.; Sajith, P. K.; Khire, S. S.; Remya, K. Host–Guest Interaction of NO and NO+species with Calixerenes: Dissecting the Impact of Conformational and Confinement Effects. *Physical Chemistry Chemical Physics* **2026**, *28* (5), 3562–3575. https://doi.org/10.1039/d5cp03650j

(36) Peintinger, M. F.; Beck, J.; Bredow, T. Charged Stacks of Dithiin, Diselenin, Thianthrene and Selenanthrene Radical Cations: Long Range Multicenter Bonds. *Physical Chemistry Chemical Physics* **2013**, *15* (42), 18702–18709. https://doi.org/10.1039/c3cp53410c

Supplementary Files

This is a list of supplementary files associated with this preprint. Click to download.

- SItca1311.pdf